SCIENCE CHINA
Life Sciences

•RESEARCH PAPER•

November 2022 Vol.65 No.11: 2287–2300
https://doi.org/10.1007/s11427-022-2157-y

PITPNC1 promotes the thermogenesis of brown adipose tissue under acute cold exposure

Guoqing Tang[1†], Chengxin Ma[1†], Liangkui Li[2], Shaoyan Zhang[1], Fengsheng Li[1], Jin Wu[1], Yesheng Yin[1], Qing Zhu[1], Yan Liang[1], Ru Wang[3], He Huang[1], Tong-Jin Zhao[1,4], Hongyuan Yang[5], Peng Li[1,2,4] & Feng-Jung Chen[1,4*]

[1]*Shanghai Key Laboratory of Metabolic Remodeling and Health, Institute of Metabolism and Integrative Biology, Institutes of Biomedical Sciences, Department of Endocrinology and Metabolism, Zhongshan Hospital, Fudan University, Shanghai 200438, China;*
[2]*State Key Laboratory of Membrane Biology and Tsinghua-Peking Center for Life Sciences, Beijing Advanced Innovation Center for Structural Biology, School of Life Sciences, Tsinghua University, Beijing 100084, China;*
[3]*School of Kinesiology, Shanghai University of Sport, Shanghai 200438, China;*
[4]*Shanghai Qi Zhi Institute, Shanghai 200030, China;*
[5]*School of Biotechnology and Biomolecular Sciences, the University of New South Wales, Sydney, NSW 2052, Australia*

Received April 9, 2022; accepted June 29, 2022; published online September 23, 2022

Brown adipose tissue (BAT) plays an essential role in non-shivering thermogenesis. The phosphatidylinositol transfer protein, cytoplasmic 1 (PITPNC1) is identified as a lipid transporter that reciprocally transfers phospholipids between intracellular membrane structures. However, the physiological significance of PITPNC1 and its regulatory mechanism remain unclear. Here, we demonstrate that PITPNC1 is a key player in thermogenesis of BAT. While *Pitpnc1*$^{-/-}$ mice do not differ with wildtype mice in body weight and insulin sensitivity on either chow or high-fat diet, they develop hypothermia when subjected to acute cold exposure at 4°C. The *Pitpnc1*$^{-/-}$ brown adipocytes exhibit defective β-oxidation and abnormal thermogenesis-related metabolism pathways in mitochondria. The deficiency of lipid mobilization in *Pitpnc1*$^{-/-}$ brown adipocytes might be the result of excessive accumulation of phosphatidylcholine and a reduction of phosphatidic acid. Our findings have uncovered significant roles of PITPNC1 in mitochondrial phospholipid homeostasis and BAT thermogenesis.

PITPNC1, thermogenesis, acute cold exposure, β-oxidation, lipid homeostasis

Citation: Tang, G., Ma, C., Li, L., Zhang, S., Li, F., Wu, J., Yin, Y., Zhu, Q., Liang, Y., Wang, R., et al. (2022). PITPNC1 promotes the thermogenesis of brown adipose tissue under acute cold exposure. Sci China Life Sci 65, 2287–2300. https://doi.org/10.1007/s11427-022-2157-y

INTRODUCTION

Adipose tissues store fat and also mobilize fat in response to a variety of environmental stress such as fasting and cold challenge (Chouchani and Kajimura, 2019; Scheele and Wolfrum, 2020). The regulatory circuits are composed of white adipose tissue (WAT) for fuel storage and brown adipose tissue (BAT) for thermogenic oxidation, and play a crucial role in systemic energy homeostasis (Chondronikola and Sidossis, 2019; Kahn et al., 2019; Kang, 2021). Dysregulation of regulatory signaling pathways in the system is closely associated with metabolic disorders including obesity, non-alcoholic fatty liver disease, type 2 diabetes, and atherosclerosis (Mulder et al., 2016; Polyzos et al., 2017; Saraswathi et al., 2020; Saxton et al., 2019). Under acute cold exposure, the sympathetic nervous system in WAT and BAT is greatly activated and norepinephrine (NE) is released from nerve terminals (Sigurdson and Himms-Hagen, 1988).

†These authors contributed equally
*Corresponding author (Feng-Jung Chen, email: derrick_chen@fudan.edu.cn)

NE binds to the β3 adrenergic receptor (β3-AR) on the plasma membrane of white or brown adipocytes and activates a downstream cyclic adenosine monophosphate/protein kinase A (cAMP/PKA) signaling pathway (Chouchani and Kajimura, 2019; Hoffmann et al., 2016). PKA phosphorylates cytosolic lipases such as adipose triglyceride lipase (ATGL) and hormone-sensitive lipase (HSL), which catalyze triglycerides (TG) and diacylglycerol (DG) to releases glycerol and non-esterified fatty acids (NEFA) especially from WAT as fuel for thermogenesis in BAT (Hücking et al., 2003; Mueez et al., 2018).

Phosphatidylinositol transfer proteins (PITP) play a key role in lipid binding and transfer by transporting phospholipids such as phosphatidylinositol (PI), phosphatidylcholine (PC), or phosphatidic acid (PA) between intracellular membrane structures (Allen-Baume et al., 2002; Cockcroft, 2001; Garner et al., 2012). Members of PITP family include PITPNA, PITPNB, PITPNC1, and PITPNM1 (Cockcroft and Garner, 2011; Hsuan and Cockcroft, 2001). *Pitpna* knockout mice exhibit aponecrotic spinocerebellar disease, hypoglycemia, and intestinal and hepatic steatosis (Alb Jr. et al., 2003). PITPNB is indispensable for COPI-mediated retrograde transport from Golgi to the endoplasmic reticulum (ER) (Carvou et al., 2010). *Pitpnm1* knockout mice are embryonic-lethal (Cockcroft, 2012) and depletion of *Pitpnm1* in cultured HeLa cells using RNAi revealed disorganized Golgi with defective protein export to the plasma membrane (Litvak et al., 2005). PITPNC1 is required for the reciprocal transfer of PA and PI between the intracellular membrane system (Garner et al., 2012; Grabon et al., 2017). Recently, PITPNC1 is found to be highly expressed in cancer cells and to facilitate cancer cell proliferation (Halberg et al., 2016; Tan et al., 2020; Tan et al., 2018). PITPNC1 recruits RAB1B to Golgi to promote the malignant secretion of pro-metastatic proteins in metastatic breast, melanoma, and colon cancers (Halberg et al., 2016). In addition, PITPNC1 promotes the fatty acid absorption and oxidation of gastric cancer cells, inducing anoikis resistance and omental metastasis (Tan et al., 2018). However, the physiological significance of PITPNC1 in whole-body metabolic homeostasis remains elusive.

We report here that PITPNC1 is enriched in adipose tissues. We generated *Pitpnc1*$^{-/-}$ mice and found that they developed hypothermia under acute cold exposure. With a combination of biochemical assays, metabolomics, lipidomics, and multiple imaging-based approaches, we found that the deficiency of lipid mobilization in the brown adipocytes of *Pitpnc1*$^{-/-}$ mice mainly results from defective β-oxidation in mitochondria. Therefore, this study reveals that PITPNC1 controls mitochondrial phospholipid composition and function, and provides insights into the significance of lipid trafficking in thermogenesis.

RESULTS

PITPNC1 is expressed in metabolic tissues

PITP family proteins are lipid transporters, consisting of PITPNA, PITPNB, PITPNM1, and the long and short forms of PITPNC1 (Figure 1A). We first checked the expression profiles of these four genes and found that all four PITPs were mainly expressed in metabolic tissues such as liver, white adipose tissue (WAT), and brown adipose tissue (BAT) (Figure 1B, Figure S1A–C in Supporting Information). We were particularly interested in *Pitpnc1*, as it was enriched in both WAT and BAT (Figure 1B). Western blot analysis showed that both long and short forms of PITPNC1 were expressed in sWAT, gWAT, and BAT, as well as liver and kidney, whereas the long form was enriched in heart and brain (Figure 1C). As PITPNC1 transfers phospholipids between organelles (Cockcroft and Garner, 2011; Cockcroft and Garner, 2012; Shadan et al., 2008), we next identify the subcellular localization of PITPNC1. Organelle fractions isolated from mouse liver showed that endogenous PITPNC1 proteins were appeared at lipid droplets (LDs), Golgi, ER, and mitochondria (Figure 1D). Besides, fluorescent imaging showed that overexpressing PITPNC1-GFP in COS7 cells mostly concentrated around LDs with the ER (Figure 1E). The results suggest that PITPNC1 might shuttle between intracellular organelles to regulate the physiological functions of the metabolic tissues.

Pitpnc1$^{-/-}$ mice show no difference in body weight and insulin sensitivity with wildtype mice under normal or high-fat diet treatment

As PITPNC1 transfers phospholipid and is mainly expressed in metabolic tissues, we next generated *Pitpnc1* whole-body knockout (*Pitpnc1*$^{-/-}$) mice using CRISPER-Cas9 technique and confirmed its knockout efficiency on both forms of PITPNC1 (Figure 2A and B, Fiugre S2A in Supporting Information). We subjected 6-week-old wildtype (WT) and *Pitpnc1*$^{-/-}$ mice to normal chow diet (ND) or high-fat diet (HFD) for 16-weeks. Figure 2C showed that there was no difference in body weight between the two genotypes under either ND or HFD. There was also no difference in fat mass (Figure 2D), lean mass (Figure 2E) or food intake (Figure 2F) between the two mouse strains. Glucose tolerance test (GTT) and insulin tolerance test (ITT) did not show much difference between the two genotypes under either diet treatment (Figure 2G and H). Blood biochemistry analysis revealed no difference in glucose and TG in serum (Figure S2B and C in Supporting Information). Tissue weights of BAT, sWAT, gWAT, or liver did not differ either (Figure S2D–G in Supporting Information). H&E images of LDs in tissues showed total LD amount and LD size in the liver,

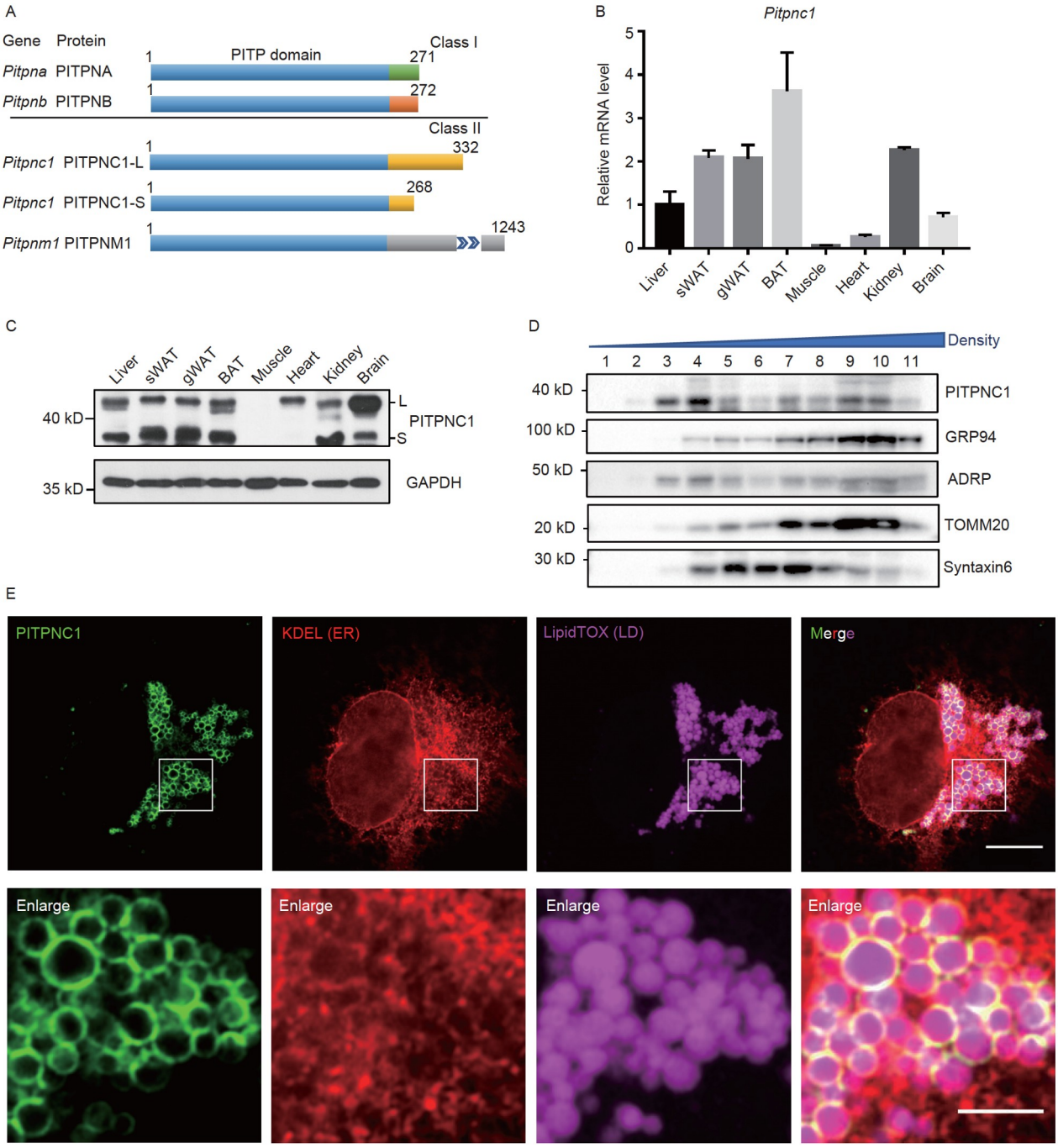

Figure 1 The expression profile and subcellular localization of PITPNC1 proteins. A, Schematic diagram of PITP family proteins, including PITPNA, PITPNB, PITPNM1, and short and long forms of PITPNC1. B, Relative mRNA levels of *Pitpnc1* in various tissues of wildtype mice. The abbreviations used are: sWAT, subcutaneous adipose tissue; gWAT, gonadal adipose tissue. C, Expression level of PITPNC1 proteins in various tissues of wildtype mice. GAPDH is a loading control. L, long form of PITPNC1; S, short form of PITPNC1. D, Subcellular fractions through sucrose density gradient centrifugation show that endogenous PITPNC1 proteins in liver were localized to various organelles such as LDs, mitochondria, ER, and Golgi. GRP94 is an ER marker; ADRP is a LD marker; TOMM20 is a mitochondria marker; Syntaxin6 is a Golgi marker. E, Fluorescent images show the subcellular localization of overexpressing PITPNC1-GFP proteins at LDs and ER. KDEL is an ER marker; LipidTOX was used to stain LDs. Scale bars, 10 μm; (Enlarge) 3 μm.

BAT, and gWAT were similar in control WT mice and *Pitpnc1*$^{-/-}$ mice (Figure S2H in Supporting Information). These data indicate that PITPNC1 deficiency does not play a role in the accumulation of lipids and the development of obesity.

Pitpnc1$^{-/-}$ mice develop hypothermia under acute cold exposure

As PITPNC1 is prominently expressed in BAT and WAT (Figure 1B), we then examined its role in thermogenesis by

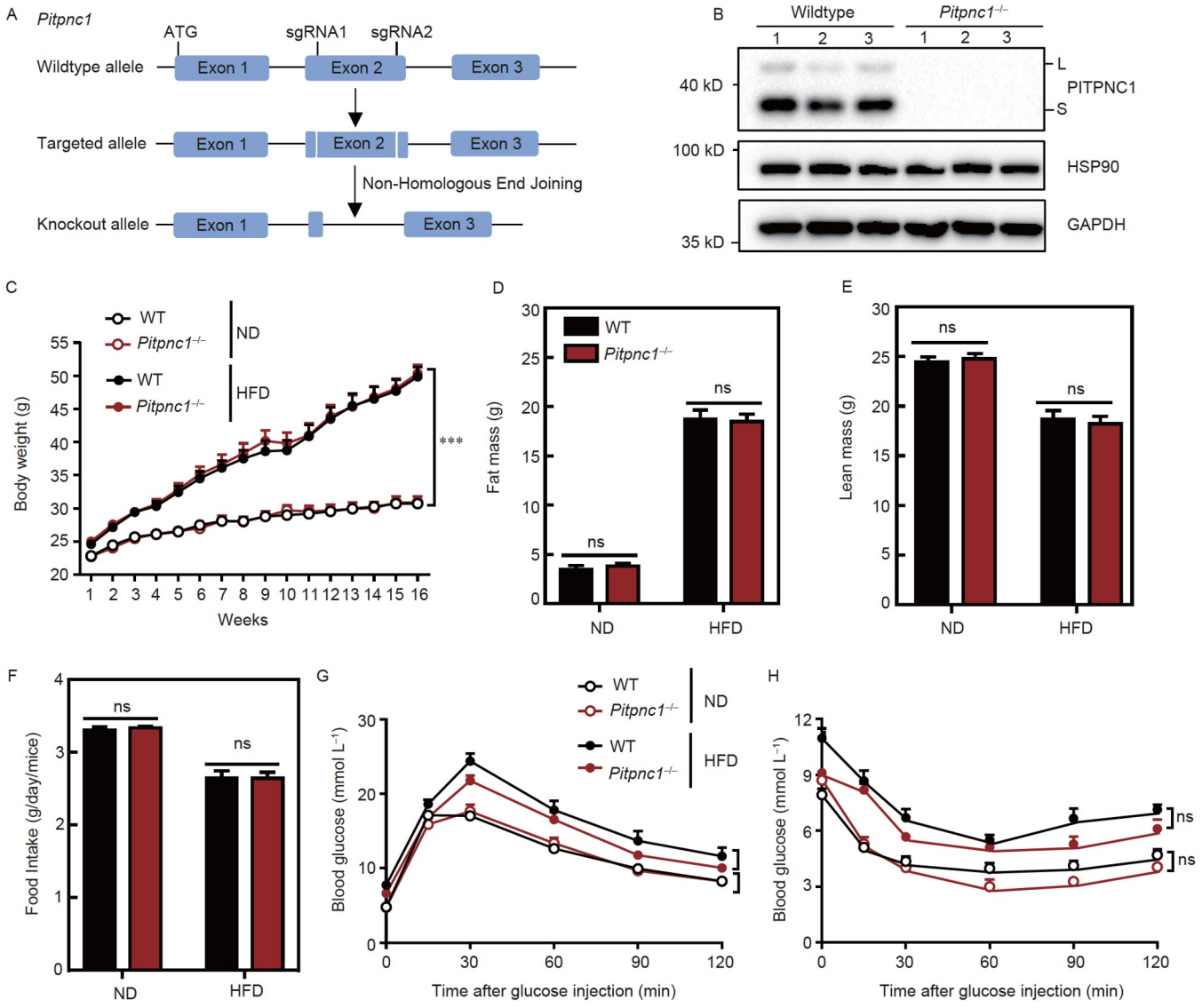

Figure 2 *Pitpnc1*$^{-/-}$ mice have no phenotype after high-fat diet treatment. A, Schematic diagram of *Pitpnc1* whole-body knockout mice construction. B, Expression level of PITPNC1 proteins in the BAT of wildtype and *Pitpnc1*$^{-/-}$ mice. C–H, Male littermates (6-week-old) of wildtype mice and *Pitpnc1*$^{-/-}$ mice were fed either normal chow diet (ND) or high-fat diet (HFD) for 16 weeks. The body weight (C), fat mass (D), lean mass (E), and food intake (F) of wildtype mice and *Pitpnc1*$^{-/-}$ mice were measured under the treatments of 16-weeks ND and HFD. The two mouse strains were subjected to a glucose tolerance test at week 8 (G), and were subjected to an insulin tolerance test at week 10 (H) as described in Methods. The blood glucose of mice was measured from tail vein at indicated times. 8–10 mice were used in each group. Mean ± SEM in (C)–(H). Two-tailed Student's *t* test in (D)–(F). One-way ANOVA, Holm-Šidák test in (C), (G), and (H).

subjecting the mice to acute cold exposure (Figure 3A). When housed at 22°C, both stains of mice maintained their body temperature around 38°C (Figure 3B). When the mice were subjected to acute cold exposure at 4°C, the WT mice could maintain their body temperature above 34°C, but the body temperature of *Pitpnc1*$^{-/-}$ mice dropped faster than WT mice and fell below 30°C after 4 h (Figure 3B). The results revealed that PITPNC1 is required for body temperature maintenance of mice under acute cold exposure.

These mice were sacrificed and their biochemical indexes in serum and tissues were measured. We found that after acute cold exposure, the serum glucose and TG in *Pitpnc1*$^{-/-}$ mice were significantly lower (Figure 3C and D), whereas serum NEFA was not significantly different between in the two genotypes (Figure 3E). These data implied that *Pitpnc1*$^{-/-}$ mice might have a defect in utilizing fatty acids for heat production. Further tissue examination in the acute cold exposure condition revealed that there was no difference in the weight of sWAT, gWAT, BAT, and liver between the two genotypes of mice (Figure S3A in Supporting Information). Interestingly, while the BAT from WT mice sank to the bottom of a tube in PBS, the BAT from *Pitpnc1*$^{-/-}$ mice floated to the top, indicating more TG content in the BAT of *Pitpnc1*$^{-/-}$ mice after acute cold exposure (Figure 3F). In-

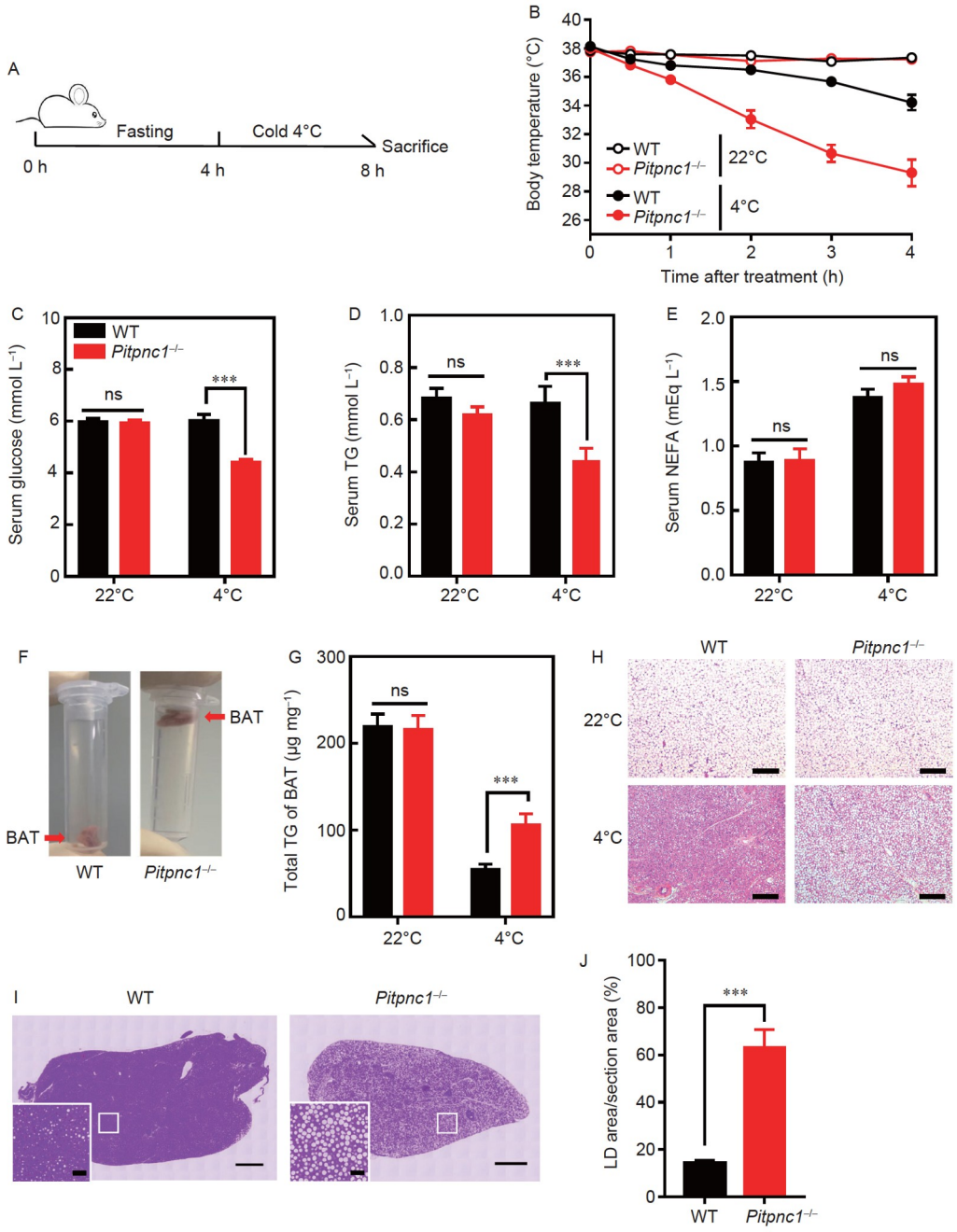

Figure 3 *Pitpnc1*$^{-/-}$ mice exhibit hypothermia under acute cold exposure. A–E, Single-housed 8-week-old male littermates of wildtype mice and *Pitpnc1*$^{-/-}$ mice were fasted for 4 h and then maintained at 22°C or switched to a 4°C cold room. Schematic diagram shows the process of acute 4°C cold exposure performed on wildtype mice and *Pitpnc1*$^{-/-}$ mice (A). The body temperatures of the two mouse strains were measured at indicated times (B). At the end of the experiment, the levels of serum glucose (C), serum triglycerides (TG) (D), and serum non-esterified fatty acid (NEFA) (E) were measured. Each value represents the mean ± SEM of 5 mice. F and G, Lipid storage in the BAT of wildtype mice and *Pitpnc1*$^{-/-}$ mice were measured and quantified. Pictures show the relative density of BAT derived from wildtype mice and *Pitpnc1*$^{-/-}$ mice after acute cold exposure (F). The TG levels in the BAT of the two mouse strains at room temperature or after acute cold exposure were measured (G). H, Representative H&E images show the lipid content in the BAT of the two mouse strains at 22°C or 4°C. Scale bars, 200 μm. I, Representative H&E images show lipid droplets (LDs) in the BAT of the two mouse strains after acute cold exposure. Scale bars, 500 μm; (Enlarge) 50 μm. J, Quantification of total LD-occupied area ratio in (I). Mean ± SEM in (B)–(E), (G), and (J). Two-tailed Student's *t* test in (C)–(E), (G), and (J). One-way ANOVA, Holm-Šidák test in (B).

deed, direct measurement showed that TG content in the BAT of *Pitpnc1*$^{-/-}$ mice was ~2-fold higher than that in control WT mice after acute cold exposure (Figure 3G). Similarly, H&E images of LDs in tissues showed that total LD amount and LD size in the liver, sWAT, and gWAT were similar in control WT mice and *Pitpnc1*$^{-/-}$ mice (Figure S3B–D in Supporting Information), but more LDs remained in the BAT of *Pitpnc1*$^{-/-}$ mice after fat expenditure under

acute cold exposure (Figure 3H). Furthermore, LD quantification analysis revealed that the surplusage of LD-occupied area ratio in the BAT of *Pitpnc1*$^{-/-}$ mice was ~3-fold more compared with control WT mice after acute cold exposure (Figures 3I and 3J). These results implied a deficiency in utilizing fatty acids in the BAT of *Pitpnc1*$^{-/-}$ mice upon acute cold exposure.

We also measured the transcriptional expression levels of several key genes in metabolic pathways such as adipogenesis, lipogenesis, lipolysis, and β-oxidation, but found no difference in the BAT of *Pitpnc1*$^{-/-}$ and WT mice (Figure S3E in Supporting Information). Similarly, we did not find any change in the expression of key proteins in the BAT between *Pitpnc1*$^{-/-}$ mice and control WT mice under acute cold exposure, especially tyrosine hydroxylase (TH), CD36, COX2/4, and UCP1 (Figure S3F in Supporting Information). These data indicated that *Pitpnc1*$^{-/-}$ mice have no defect in the signal transduction from activation of sympathetic nerves to cAMP/PKA signaling in brown adipocytes.

Pitpnc1$^{-/-}$ brown adipocytes exhibit decreased mitochondrial β-oxidation activity

We directly examined the cAMP/PKA signaling pathway in BAT by using CL316,243, a β3-adrenergic receptor agonist, and found that the activation of phosphorylated AKT and phosphorylated HSL between *Pitpnc1*$^{-/-}$ and control WT mice were not different (Figure 4A). To further characterize the role of PITPNC1 in the metabolic processes of brown adipocytes (Figure 4B), we isolated primary stromal vascular fraction (SVF) cells from the BAT of WT mice and *Pitpnc1*$^{-/-}$ mice and differentiated them into mature brown adipocytes. We first performed immunostaining to examine the subcellular localization of CD36, a key player in fatty acid uptake in adipocytes (Glatz and Luiken, 2018; Hao et al., 2020; Wang et al., 2019), and found that CD36 was normally localized to the plasma membrane of both types of brown adipocytes (Figure S4A in Supporting Information). We then examined fatty acid uptake and storage in WT and *Pitpnc1*$^{-/-}$ brown adipocytes by recording the time-lapse images of growing LDs for 4 h. Both types of brown adipocytes were able to accumulate and to store TGs in LDs over time and there was no difference in the rate and amount of TG accumulation between the two genotypes of cells (Figure S4B in Supporting Information). We next examined lipolysis in these cells by treating cells with isoproterenol and recording the time-lapse images of degradable LDs for 4 h, and found that reduced LD volume over time was similar in the two types of cells (Figure S4C in Supporting Information). Furthermore, glycerol release from control WT brown adipocytes and *Pitpnc1*$^{-/-}$ brown adipocytes to medium was similar (Figure S4D in Supporting Information). We then switched to analyze the mitochondrial β-oxidation activity by monitoring the oxygen consumption rate (OCR). We found that the basic and maximum OCR of *Pitpnc1*$^{-/-}$ brown adipocytes were lower compared with that of control WT brown adipocytes (Figure 4C).

To further confirm the results, we purified mitochondria from BAT (Figure 4D). We found that the OCR of mitochondria derived from the BAT of *Pitpnc1*$^{-/-}$ mice was significantly lower (Figure 4E). As a control, we measured the activity of citrate synthase (Zhou et al., 2020) to make sure equal numbers of purified mitochondria were used (Figure 4F). We did not find much difference in mitochondrial DNA content or mitochondrial morphology in BAT by electron microscopy (EM) between WT mice and *Pitpnc1*$^{-/-}$ mice (Figure S4E and F in Supporting Information). Further quantification of mitochondrial morphology in EM images showed that there was no difference in mitochondria number, mitochondrial cristae number, and the sectional area, perimeter, and shape of mitochondria in the BAT between the two mouse strains (Figure S4G–K in Supporting Information). In addition, the mitochondrial proteins, including COX4, CPT1B, TOMM20, and UCP1 did not show any difference either (Figure 4G), suggesting that the defect in mitochondrial β-oxidation in *Pitpnc1*$^{-/-}$ brown adipocytes is not due to dysfunctional mitochondrial proteins.

Knockout of *Pitpnc1* disrupts lipid homeostasis of BAT mitochondria

The role of PITPNC1 in lipid transfer intrigued us to assess lipid variations within the mitochondria of *Pitpnc1*$^{-/-}$ brown adipocytes. We performed the refined purification of mitochondria for lipidomics and ensured that there was no contamination of mitochondria with other organelles (Figure 5A and B). The principal component analysis showed that major lipid components in the mitochondria purified from the BAT of control WT mice and that of *Pitpnc1*$^{-/-}$ mice were significantly different (Figure 5C). Compared with the control groups, several lipids such as PC, sphingomyelin (SM), and ceramide (Cer) were up-regulated, whereas some lipids including PA were down-regulated in BAT of *Pitpnc1*$^{-/-}$ mice (Figure 5D, F–H). According to the lipid remodeling pathway (Figure 5E), the series of turnover lipids from PC to ceramide were entirely increased within the mitochondria purified from *Pitpnc1*$^{-/-}$ BAT (Figure 5D–G). Importantly, ceramide accumulation was known to cause deficient mitochondrial β-oxidation (Chaurasia et al., 2021; Chaurasia et al., 2016; Zhang et al., 2019). These results suggest that the excessive accumulation of ceramides results in the defective mitochondrial function of *Pitpnc1*$^{-/-}$ BAT. In addition, metabolomic analysis revealed the defective pyrimidine metabolism and purine metabolism in the BAT of *Pitpnc1*$^{-/-}$ mice (Figure S5 in Supporting Information). The levels of key metabolites such as glutamine, carbamoyl

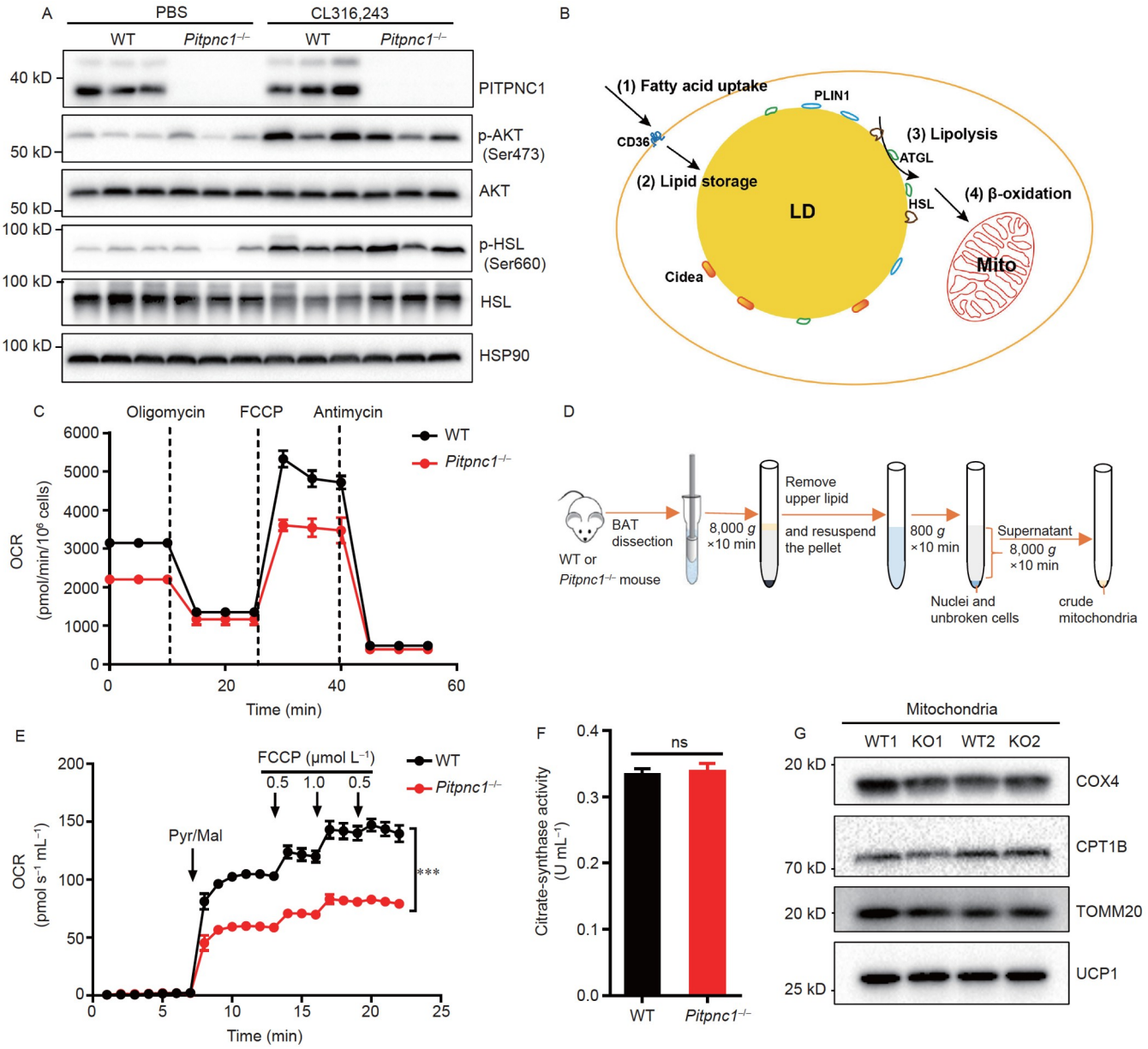

Figure 4 Adipocytes derived from the BAT stromal vascular fraction (SVF) cells of *Pitpnc1*$^{-/-}$ mice lose the β-oxidation activity of mitochondria. A, Expression level of indicated proteins in the BAT of wildtype mice and *Pitpnc1*$^{-/-}$ mice after injection of PBS or CL316,243. B, Schematic diagram shows the processes of lipid metabolism in brown adipocytes such as fatty acid uptake, lipid storage, lipolysis, and β-oxidation. C, Oxygen consumption rate (OCR) of mature adipocytes derived from the BAT SVF cells of the two mouse strains. D, Schematic diagram shows the process of mitochondria purification from the BAT of the two mouse strains. E–G, The OCR (E), citrate-synthase activity (F), and expression level of indicated proteins on the outer or inner membrane (G) of mitochondria purified from the BAT of the two mouse strains in (D) were measured. Mean ± SEM in (C), (E), and (F). Two-tailed Student's *t* test in (F). One-way ANOVA, Holm-Šidák test in (C) and (E).

phosphate, aspartate, and NADH in the pyrimidine metabolism pathway (Figure S5D and E in Supporting Information) and adenosine, inosine, hypoxanthine, and xanthine in the purine metabolism pathway were lower for the BAT of *Pitpnc1*$^{-/-}$ mice (Figures S5D and F in Supporting Information). The pyrimidine metabolism and purine metabolism pathways are highly correlated with thermogenesis (Bast-Habersbrunner and Fromme, 2020; Fromme et al., 2018; Macher et al., 2018). Besides, to examine how the conversion from PC to ceramide enhances, we measured the transcriptional expression levels of two key enzymes, namely sphingomyelin synthases (*Sgms1*) for PC or ceramide to SM and sphingomyelinases (*Smpd3*) for SM to ceramide. The results showed that their relative mRNA levels were slightly but not effectively different in the BAT between the two mouse strains (Figures S6A and B in Supporting Information). We speculate that the PC increment possibly leads to the series of increased lipids such as SM and ceramide within the mitochondria of *Pitpnc1*$^{-/-}$ BAT. From these results shown above, we hypothesize that

PITPNC1 might exchange PC and PA molecules between mitochondria and other organelles by transporting PC away from mitochondria and PA to mitochondria. Ablation of *Pitpnc1* blocks the phospholipid exchange and results in elevated PC in mitochondria. PC then gets converted to ceramide, which leads to dysfunction of mitochondrial β-oxidation and thermogenesis (Figure 5I).

DISCUSSION

In recent years, PITPNC1 was found to play an important role in tumor proliferation and metastasis (Ashlin et al., 2018; Halberg et al., 2016; Tan et al., 2020; Tan et al., 2018). Here, we identify a novel physiological role of PITPNC1 in adaptive thermogenesis. We found that *Pitpnc1*$^{-/-}$ mice developed hypothermia under acute cold exposure. *Pitpnc1*$^{-/-}$ BAT exhibited the deficiency of utilizing fatty acids but had no defect in sympathetic nervous system and cAMP/PKA signaling pathway. On the other hand, glucose is another energy supply for BAT thermogenesis (Chitraju et al., 2020). After acute cold exposure, the serum glucose in *Pitpnc1*$^{-/-}$ mice was significantly lower compared with wildtype mice. The result indicates that *Pitpnc1*$^{-/-}$ mice normally utilized serum glucose for heat production. Mechanistically, the dysfunctional mitochondrial β-oxidation in the brown adipocytes of *Pitpnc1*$^{-/-}$ mice may result from abnormal mitochondrial lipid homeostasis, namely excessive accumulation of PC and ceramides. Growing evidence has shown that mitochondrial phospholipid disorders lead to mitochondrial diseases, which is different from most past cases in which the deficiency of protein machinery in mitochondria was only addressed (Hernández-Alvarez et al., 2019; Li et al., 2020). It was found that the accumulation of $C_{16:0}$ ceramides in mitochondria inhibits β-oxidation by recruiting mitochondrial fragmentation factor (MFF) (Hammerschmidt et al., 2019; Li et al., 2020; Turpin et al., 2014). Our lipidomic analysis also found this similar increment of $C_{16:0}$ ceramides in BAT mitochondria of *Pitpnc1*$^{-/-}$ mice. As the activation of thermogenesis was proposed to be a new therapeutic strategy for the treatment of obesity (Cheng et al., 2021; Stephens et al., 2011; Ye et al., 2021), optimizing mitochondrial lipid homeostasis by targeting lipid transporters including PITPNC1 may be a viable approach in developing anti-obesity therapies.

Another interesting issue is the regulatory mechanism in thermogenesis by which PITPNC1 controls the level of mitochondrial PC and PA molecules possibly by exchanging them between mitochondria and other organelles. Some studies have revealed that PITPNC1 binds and transfers PA, PC, and PI molecules, while PITPNA and PITPNB are responsible for the transfer of PI or PC molecules as previously described (Cockcroft and Garner, 2011; Garner et al., 2012). Besides, to estimate any compensatory response from the other PITP members, we measured their transcriptional expression levels under different diet treatment or at different temperature. The results show that their mRNA levels did not differ between the two mouse strains under either diet treatment (Figure S6C and D in Supporting Information) or at either temperature (Figure S6E and F in Supporting Information). The results suggest that there could be no compensation in thermogenesis by the other PITP members in the *Pitpnc1*$^{-/-}$ mice under acute cold exposure. There might be unique functional motifs in PITPs for their targeting to various organelles, because there is only 40% homology in amino acid sequence of PITPNC1 compared with other PITPs (Cockcroft and Garner, 2011). It would be interesting to figure out how each of the PITP members shuttles between different organelles to maintain phospholipid homeostasis.

In summary, we have uncovered a role of PITPNC1 in the mitochondrial lipid homeostasis and β-oxidation of BAT, as well as a new mechanism to control thermogenesis. Such regulation of phospholipid homeostasis may be a prototype for other lipid transporters that mediate organelle communications to preserve their biological functions. The current study is technically limited by the difficulty of lipid transfer and binding reconstitution experiments with *in vitro* synthesized liposomes and recombinant full-length PITPNC1 proteins. Future investigations will focus on addressing the exact role of PITPNC1 in controlling mitochondrial lipid homeostasis and function.

MATERIALS AND METHODS

Resource availability

Lead contact

Further information and requests for resources and reagents should be directed to and will be fulfilled by the lead contact, Dr. Feng-Jung Chen (derrick_chen@fudan.edu.cn).

Materials availability

All reagents generated for this paper are available upon reasonable request.

Data and code availability

All data reported in this paper will be shared by the lead contact upon request. This paper does not report original code. Any additional information required to reanalyze the data reported in this work paper is available from the Lead Contact upon request.

Experimental model and subject details

Mice

All animal procedures were approved by the Institutional

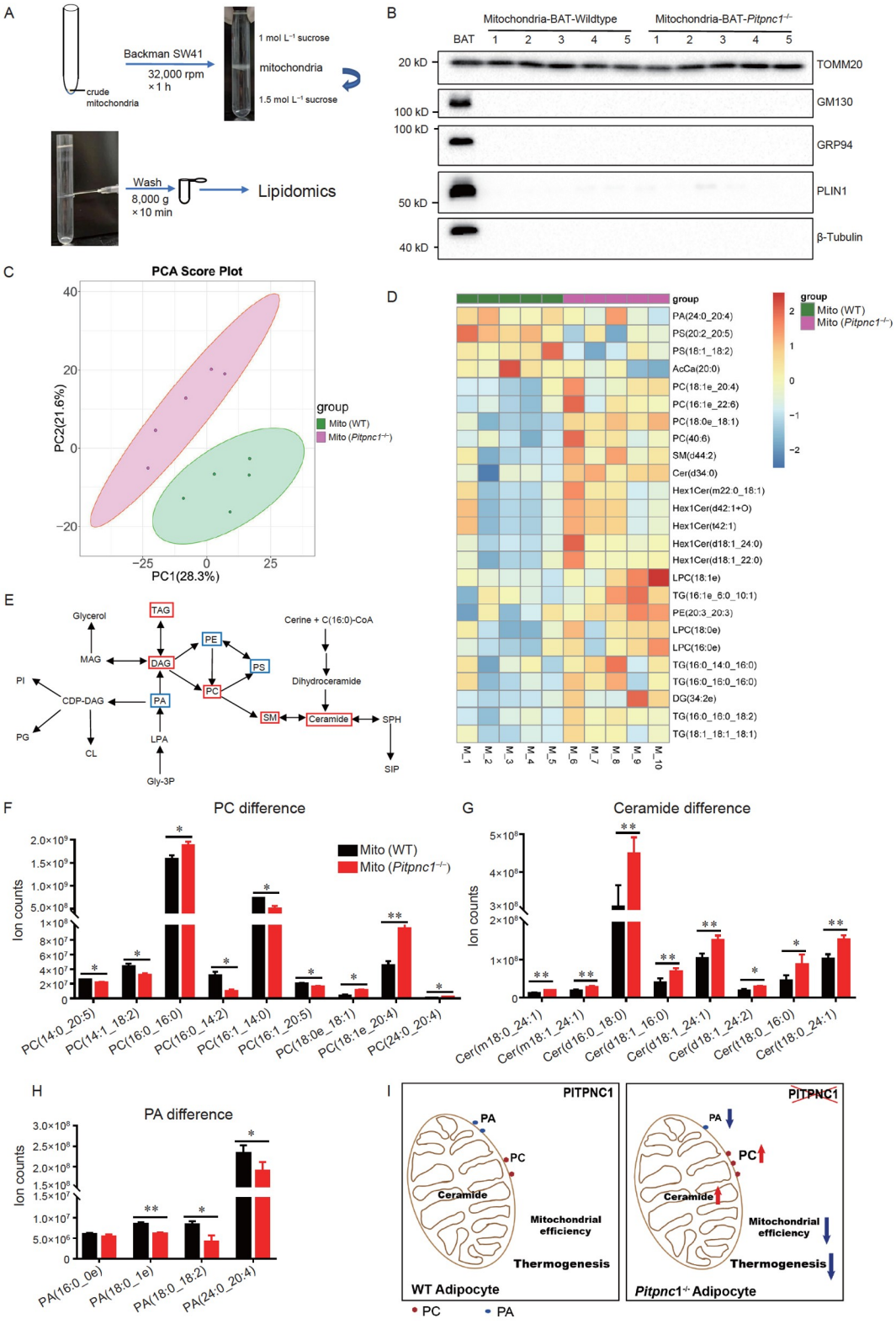

Figure 5 Lipidomics shows variation of individual lipids in mitochondria derived from the BAT of *PITPNC1*$^{-/-}$ mice. A, Schematic diagram shows the post-purification process of crude mitochondria for lipidomics. B, Western blot analysis shows there was no other organelle contamination in mitochondrial factions. TOMM20 is a mitochondria marker; GM130 is a Golgi marker; GRP94 is an ER marker; PLIN1 is a LD marker. C and D, PCA score plot (C) and hierarchical clustered heatmaps (D) of two lipidomic datasets derived from the purified mitochondria from the BAT of control wildtype and *Pitpnc1*$^{-/-}$ mice in (B). E, Schematic diagram shows variation of the two lipidomic datasets of mitochondria in (B). F–H, Phosphatidylcholine (PC) difference (F), ceramide difference (G), and phosphatidic acid (PA) difference (H) in the two lipidomic datasets of mitochondria in (B) were calculated and summarized. I, Model shows that PITPNC1 regulates mitochondrial lipid homeostasis in brown adipocytes under acute cold exposure. Mean ± SEM in (F)–(H). Two-tailed Student's *t* test in (F)–(H).

Ethics Committee of Fudan University, under a permit of animal use in the Center of Experimental Animal at Shanghai. The permit followed the Experimental Animal Regulations set by the National Science and Technology Commission, China. All mice were housed in the animal facility with a 12 h light/dark cycle, the temperature at 22°C–23°C and the relative humidity at 60%, with free access to standard chow and water.

The chow diet (Xietong Organism, Nanjing, China) contains 3.65 kcal g^{-1} of metabolizable energy, of which 12% of calories are from fat, 67.4% from carbohydrates, and 20.6% from protein. The high-fat diet (HFD, Research Diet, #D12492) contains 60% calories from fat, 20% calories from carbohydrate and 20% calories from protein.

Pitpnc1 knockout (*Pitpnc1*$^{-/-}$) mice were generated at laboratory animal center of Tsinghua University using the CRISPR-Cas9 system. Briefly, two guide RNAs of mouse *Pitpnc1* (gRNA1: caccgcgtgcagaacgagccctttg; gRNA2: aaaccaaagggctcgttctgcacgc) were designed to achieve a deletion of exon2. Transcribed guide RNAs and Cas9 were injected into C57BL/6J fertilized eggs.

In either case, the mutated protein will not be functional as it lacks the PITP functional motif. Genotyping was performed by the following primers: Forward, GTTCTGCAGTACAAAATC GGAC; Reverse, GGTGGCATAATGGCTTTCTAGTG. The amplicons of WT and knockout alleles are 231 and 172 bp, respectively.

Cell culture and treatment

Cos7 cells were cultured in Dulbecco's modified Eagle's medium (DMEM; Invitrogen, USA) containing 10% fetal bovine serum (FBS; Invitrogen, USA), 100 U mL^{-1} penicillin and 100 μg mL^{-1} streptomycin at 37°C in a humidified incubator containing 5% CO_2. To promote the formation of LDs in specific experiments, cells were treated with sodium oleate (OA; Sigma, USA) conjugated to fatty acid-free BSA and added to the culture medium to give a final concentration of 200 μmol L^{-1}. Plasmid DNAs were transfected into Cos7 cells using Lipofectamine 2000 according to manufacturer's instruction (Invitrogen, USA).

Mature brown adipocytes were cultured in growth medium at 37°C in a humidified incubator containing 5% CO_2. The growth medium is Dulbecco's modified Eagle's medium (DMEM) containing 1% penicillin/streptomycin, 20 mmol L^{-1} HEPES (Life Technologies, catalog #15630-080), and 20% fetal bovine serum (FBS, Invitrogen, USA). To promote the growth of LDs in specific experiments, mature brown adipocytes were treated with sodium oleate (OA; Sigma, USA) or other fatty acids conjugated to fatty acid-free BSA and added to the culture medium to give a final concentration of 200 μmol L^{-1}.

Method details

Plasmids construction

Full-length cDNAs encoding various mouse proteins were amplified by PCR from cDNAs of mouse liver or brown adipose tissue. cDNA encoding mouse PITPNC1 was cloned into pEGFP-C1 (Clontech) or pEGFP-N1 (Clontech) vectors.

RNA extraction and real-time PCR

Total RNA was extracted from diverse cells or mice tissues with Triazole reagent (Invitrogen, USA). The first-strand cDNA synthesis was performed with PrimeScript RT reagent Kit with gDNA Eraser (Takara, Japan). Real-Time PCR reaction was performed with the SYBR Green PCR system (Applied Biosystems, USA) in an ABI Q5 thermal cycler (Applied Biosystems, USA). β-actin was used as a reference gene. The primer sequences used are listed in Table S1 in Supporting Information. The RT-qPCR data were normalized according to geometric averaging of multiple internal control genes. Analysis of raw data and calculation of normalized relative quantities were performed by the $2^{-\Delta\Delta Ct}$ method.

Western blot analysis

For western blot analysis, protein lysates were digested by IP buffer (20 mmol L^{-1} Tris, pH 7.4, 150 mmol L^{-1} NaCl, 1% Triton X-100, 1 mmol L^{-1} EDTA, and 1 mmol L^{-1} EGTA), PMSF and cocktail (Roche) using protease inhibitors. The total protein concentration was established using a BCA Protein Assay Kit (Beyotime, China). Equal amounts of protein lysates (10 to 30 μg) were separated using 10% SDS-PAGE, and transferred to PVDF membranes with a diameter of 0.45 μm. Membranes were blocked using a blocking buffer (5% BSA in TBS containing 0.1% Tween-20) and incubated overnight at 4°C with a primary antibody. Wash three times using TBS-T. Secondary HRP conjugated antibodies (1:5000, CST) were used to interact with the primary antibody under room temperature for 1 h, followed by the detection of the blots under the ECL-plus system.

Isolation of ER, Golgi, and LD fractions

Subcellular fractionation was performed as previously described (Gusarova et al., 2003). Livers were rapidly homogenized with a loose-fitted Dounce homogenizer in 5 mL of ice-cold solution containing 10 mmol L^{-1} HEPES, pH 7.4, 150 mmol L^{-1} sucrose, 0.5 mmol L^{-1} DTT, and 1× EDTA-free protease inhibitors cocktails (Roche). The homogenates were centrifuged at 1,900×*g* for 10 min at 4°C, and the supernatants were centrifuged at 100,000×*g* for 90 min at 4°C by a Beckman SW60 rotor accordingly. Then the pellets were re-suspended in 2.3 mL of an 8.58% (w/v) sucrose solution and loaded on top of a sucrose density gradient

containing the following layers (from the bottom): 56% (0.46 mL), 50% (0.92 mL), 45% (1.38 mL), 40% (2.3 mL), 35% (2.3 mL), 30% (1.38 mL), and 20% (0.46 mL) sucrose. After ultracentrifugation at 39,000 r min^{-1} for 18 h at 4°C using a Beckman SW41 rotor, 11 fractions were unloaded from top to bottom of each centrifuge tube. The distribution patterns of the subcellular compartment markers were determined by immunoblotting (ER marker: GRP94; Golgi apparatus marker: Syntaxin6; LD marker: ADRP; Mito marker: TOMM20). All procedures were performed at 4°C, and protease inhibitors cocktails were added.

Hematoxylin-eosin (H&E) staining

2.5% Avertin (150 μL/10 g) was used to anesthetize the mice by intraperitoneal injection at a specific time of experiments. Using 4% paraformaldehyde (PFA) at pH 7.4, the mice were perfused slightly until their bodies became stiff. The tissue was grasped and put into neutral 4% paraformaldehyde for 72 h. The sections of the tissue were stained with H&E according to standard procedures.

Immunofluorescent staining

Procedures for immunofluorescent staining were similar as previously described (Xu et al., 2018). Cos7 cells were cultured on coverslips within a 6-well plate or 12-well plate. When the cells grown about 50 percent at plates, transfected with 1 μg indicated plasmids for 24 h, and treated by 200 μmol L^{-1} OA for 16 h. Besides, mature brown adipocytes were cultured on coverslips within a 6-well plate or 12-well plate. These cells were rinsed twice in PBS, fixed with 4% PFA for 30 min under room temperature, permeabilized with 0.1% TritonX-100 in PBS for 10 min under room temperature, and blocked with 1% BSA in PBS for 1 h. The cells were incubated with a primary antibody (1:100–1:500 diluted) at room temperature for 2 h or at 4°C overnight, washed three times with PBS, and incubated with fluorescently labeled secondary antibody (1:1,000 diluted) for 1 h, followed by Hoechst 33342 (1:1,000 diluted) and/or Bodipy 493/503 (1:200 diluted) for nucleus and lipid droplets as indicated. LipidTOX (1:300 diluted) were also indicating lipid droplets. Coverslips contained the post-strained cells were mounted after three times washing with PBS. Images for protein localization in cells were acquired under an LSM880 confocal microscope (Carl Zeiss, German) with a 63× oil immersion objective.

Glucose and insulin tolerance tests

Glucose (GTT) and insulin (ITT) tolerance tests were carried out on 14-16-week-old control wildtype and *Pitpnc1*$^{-/-}$ mice that were fed a normal chow diet and a high-fat diet. Animals were fasted 16 h for GTT and 4 h for ITT experiments, respectively. Mice were injected intraperitoneal with glucose (GTT, chow diet 1.0 g kg^{-1} and HFD 1.5 g kg^{-1} in body weight) and recombinant human insulin (ITT, chow diet 0.5 unit kg^{-1} and HFD 1 unit kg^{-1} in body weight). Blood samples from the tail tip were collected at indicated time points and blood glucose levels were measured according to the manufacturer's instruction (ACCU-CHEK Performa (Roche)).

Acute cold exposure

Mice were maintained at 25°C. On the day of experiment, single-housed mice were briefly fasted for 4 h and then switched to a cold room at 4°C. Core temperature were measured at 0, 0.5, 1, 2, 3, and 4 h after cold exposure using a digital thermometer with a rectal thermocouple probe.

Isolation and primary culture of brown fat preadipocytes

Interscapular brown fat pad was obtained from 2-day-old C57BL/6J mice. BAT was minced and digested for 40 min at 37°C with isolation buffer and collagenase (1.5 mg mL^{-1}) (Collagenase A, B&M Roche, catalog #103,578) in PBS (1:1), vertex 10 s/5 min. Filter digested tissue through 100 μm filters into fresh, autoclaved Eppendorf vials. Centrifuge Eppendorf vials under room temperature at 1500 r min^{-1} for 5 min. Remove supernatant and re-suspend pellet in 1 mL growth medium (DMEM containing 1% penicillin/streptomycin, 20 mmol L^{-1} HEPES (Life Technologies, catalog #15630-080), and 20% FBS). Culture cells in 6 cm cell culture plates. Twenty-four hours after isolation primary cell change medium and about forty-eight hours do cell passage in differentiation medium (growth medium add 1 nm Triiodothyronine (T3, Sigma, catalog #T-2877) and 0.1 μg mL^{-1} insulin). After 4 days of differentiation, primary adipocytes were grown to confluence (37°C, 5% CO_2) followed by induction medium (differentiation medium add 5 μmol L^{-1} dexamethasone (Sigma, catalog #D-1756), 0.125 mmol L^{-1} indomethacin (Sigma, catalog #I-7378), and 0.5 mmol L^{-1} IBMX (Sigma, catalog #I-5879) for 2 days. Then re-change medium to differentiation medium for 2 days getting mature BAT primary adipocytes.

Size measurement of lipid droplets

Images of cells transfected with the indicated fluorescent vectors were randomly acquired under an LSM880 confocal microscope with Airyscan mode. Quantitative analysis of LD size in Cos7 cells and adipocytes was performed using Image J (NIH, USA). For quantitative analysis of cells containing large LDs, plasmids DNA were transfected into cells and incubated with 200 μmol L^{-1} oleic acid complexed to albumin for 24 h, fixed, and stained with Bodipy 493/503. At least 20 cells were analyzed in each set of experimental conditions.

Measurement of uptake and lipolysis rates

For uptake assay of mature adipocytes, 8-days differentiated

brown adipocytes were washed three times with PBS and then fasting 4 h in serum-free medium, then replace new serum-free medium with 200 μm OA. Bodipy 493/503 (1:200 diluted) and Hoechst 33342 (1:1,000 diluted) were respectively markers of lipid droplet and nucleus. Images for LD localization and size change in cells were acquired under high-content imaging (Opera Phenix, Perkin Elmer, America).

For lipolysis assay of mature adipocytes in image, 8-days differentiated brown adipocytes were washed three times with PBS and replace new medium with 10 μmol L^{-1} isoproterenol, then the nucleus, LD straining and image getting as the same as upper.

For lipolysis assay of mature adipocytes in glycerol release, 8-days differentiated brown adipocytes were washed three times with PBS and then incubated in phenol red-free, serum-free DMEM (Gibco) containing 1% fatty acid-free BSA (Sigma-Aldrich) in the presence or absence of 10 μmol L^{-1} isoproterenol for 4 h. The amount of glycerol released into culture medium was measured by free glycerol reagent (Sigma-Aldrich).

Isolation of mitochondria

Mitochondria isolation was performed as previously described (Zhou et al., 2020). Briefly, BAT was dissected and rinsed in ice-cold mitochondrial isolation buffer (MIB) containing 70 mmol L^{-1} sucrose, 210 mmol L^{-1} mannitol, 5 mmol L^{-1} MOPS, 5 mmol L^{-1} KH2PO4, 1 mmol L^{-1} EGTA and 0.5% (w/v) fatty acid free BSA, pH 7.2. Then tissues were homogenized with a 5-mL glass homogenizer about 20 times (up and down cycles) and transferred to a new tube. The homogenate was centrifuged at 8,000×*g* for 10 min at 4°C. Supernatant containing the lipid fraction (top) was removed and the pellet was resuspended in isolation buffer and transferred to a new tube. The supernatant was then centrifuged at 800×*g* for 10 min at 4°C to remove nuclei and cell debris. The supernatant enriched in mitochondria was then centrifuged at 8,000×*g* for 10 min at 4°C. Finally, crude mitochondrial fraction was resuspended in a small volume of MIB buffer. All the chemicals were obtained from Sigma.

Oxygen consumption rate (OCR)

OCR assay was performed as previously described (Zhou et al., 2020). OCR was determined at 37°C using the OROBOROS Oxygraph-2K module (OROBOROS Instruments GmbH). Isolated mitochondria from BAT were resuspended in respiration buffer (107.5 mmol L^{-1} KCl, 5 mmol L^{-1} K_2HPO_4, 50 mmol L^{-1} MOPS, 1 mmol L^{-1} EGTA, 1.5 mmol L^{-1} $MgCl_2$, and 0.1% w/v fatty acids-free BSA, pH 7.2). The following respiratory parameters were measured: basal respiratory rate was determined with the substrates (5 mmol L^{-1} pyruvate and 0.1 mmol L^{-1} malate), and the maximal respiratory rate was determined by increasing the concentration of carbonyl cyanide p-trifluoromethoxyphenylhydrazone (FCCP, Sigma) from 0.5 to 2 μmol L^{-1}.

Electron microscopy (EM) imaging and quantification of mitochondria in EM images

Mice were anesthetized and perfused with 2.5% glutaraldehyde, 4% formaldehyde in 0.1 mol L^{-1} phosphate buffer. The brown adipose tissue of mice was dissected, cut into small pieces, and fixed at 4°C in 2.5% glutaraldehyde, 4% formaldehyde in 0.1 mol L^{-1} phosphate buffer overnight. The tissues were rinsed in cacodylate buffer and fixed in 1% osmium tetroxide and 2% uranyl acetate for 2 h. The samples were then dehydrated in a graded ethanol series (50%, 70%, 85%, 95%, 100% × 2) for 10 min in each step. The fixed tissues were washed with acetone 3 times for 15 min and infiltrated with Embed resin (Epon812, DDSA, NMA, DMP30) at the Center of Biomedical Analysis, Tsinghua University. After incubating at 60°C for 48 h, blocks were sectioned using an ultramicrotome (Leica EM UC7) to obtain 70 nm sections. Samples were stained with uranyl acetate/lead citrate and high-resolution electron micrographs were acquired with transmission electron microscope (HITACHI H-7650B, Japan) operating at 80 kV.

All captured EM images of organelles including mitochondria and LDs in sectional BAT samples were adjusted in parallel to a similar brightness level or contrast through ImageJ (NIH). Modified images were used for quantification of mitochondrial morphology by manual measurement in ImageJ. The quantified parameters of morphological features are mitochondrial number per cell, mitochondrial cristae number, the sectional area of a mitochondrion (A), the perimeter of a mitochondrion (S), and mitochondrial shape using the simple ratio of square of mitochondrial perimeter to mitochondrial sectional area, namely S^2/A.

Quantification and statistical analysis

Data were subjected to statistical analysis in GraphPad 8.0 and plotted by Mathematica (Wolfram Research, Inc., USA) and AI Illustrator (Adobe, Inc., USA). Manual measurement of LD sizes was performed using ImageJ, statistically calculated in GraphPad 8.0, and plotted by AI Illustrator. Results represent the mean ± SEM or median with an interquartile range of at least three independent experiments as indicated in figure legends. *P* values lower than 0.05 were considered significant. Significance was established using a two-tailed Student's *t* test for two-group comparison. For multiple comparison, one-way ANOVA with a post-hoc Holm-Šidák test was utilized with the *P*-values multiplicity adjusted. Statistical difference was shown as $*P<0.05$, $**P<0.01$, and $***P<0.001$. ns represents no significant difference.

Compliance and ethics *The author(s) declare that they have no conflict of interest. All applicable institutional and/or national guidelines for the care and use of animals were followed.*

Acknowledgements *This work was supported by the National Key R&D Program of China (2018YFA0506900), the National Natural Science Foundation of China (91857103), the National Key R&D Program of China (2018YFA0800301), Shanghai Basic Research Field Project "Science and Technology Innovation Action Plan" (21JC1400400), the Lingang Laboratory (LG-QS-202204-06), and Shanghai Municipal Science and Technology Major Project (2017SHZDZX01). We would like to thank the members of the P.L. laboratory at Fudan University for technical assistance and productive discussions; Ms. Ke Qiao and Ms. Na Wei at the Imaging Core Facility of IMIB at Fudan University for the fluorescent and H&E imaging supporting; Ms. Ke Qiao, Ms. Lanlan Zhang, and Ms. Hongfang Zhao for metabolomic and lipidomic data generation from the Single Cell Quantitative Metabolomics and Lipidomics Core Facility of IMIB at Fudan University.*

References

Alb Jr., J.G., Cortese, J.D., Phillips, S.E., Albin, R.L., Nagy, T.R., Hamilton, B.A., and Bankaitis, V.A. (2003). Mice lacking phosphatidylinositol transfer protein-α exhibit spinocerebellar degeneration, intestinal and hepatic steatosis, and hypoglycemia. J Biol Chem 278, 33501–33518.

Allen-Baume, V., Ségui, B., and Cockcroft, S. (2002). Current thoughts on the phosphatidylinositol transfer protein family. FEBS Lett 531, 74–80.

Ashlin, T.G., Blunsom, N.J., Ghosh, M., Cockcroft, S., and Rihel, J. (2018). Pitpnc1a regulates zebrafish sleep and wake behavior through modulation of insulin-like growth factor signaling. Cell Rep 24, 1389–1396.

Bast-Habersbrunner, A., and Fromme, T. (2020). Purine nucleotides in the regulation of brown adipose tissue activity. Front Endocrinol 11, 118.

Carvou, N., Holic, R., Li, M., Futter, C., Skippen, A., and Cockcroft, S. (2010). Phosphatidylinositol- and phosphatidylcholine-transfer activity of PITPβ is essential for COPI-mediated retrograde transport from the Golgi to the endoplasmic reticulum. J Cell Sci 123, 1262–1273.

Chaurasia, B., Ying, L., Talbot, C.L., Maschek, J.A., Cox, J., Schuchman, E.H., Hirabayashi, Y., Holland, W.L., and Summers, S.A. (2021). Ceramides are necessary and sufficient for diet-induced impairment of thermogenic adipocytes. Mol Metab 45, 101145.

Chaurasia, B., Kaddai, V.A., Lancaster, G.I., Henstridge, D.C., Sriram, S., Galam, D.L.A., Gopalan, V., Prakash, K.N.B., Velan, S.S., Bulchand, S., et al. (2016). Adipocyte ceramides regulate subcutaneous adipose browning, inflammation, and metabolism. Cell Metab 24, 820–834.

Cheng, L., Wang, J., Dai, H., Duan, Y., An, Y., Shi, L., Lv, Y., Li, H., Wang, C., Ma, Q., et al. (2021). Brown and beige adipose tissue: a novel therapeutic strategy for obesity and type 2 diabetes mellitus. Adipocyte 10, 48–65.

Chitraju, C., Fischer, A.W., Farese Jr., R.V., and Walther, T.C. (2020). Lipid droplets in brown adipose tissue are dispensable for cold-induced thermogenesis. Cell Rep 33, 108348.

Chondronikola, M., and Sidossis, L.S. (2019). Brown and beige fat: from molecules to physiology. Biochim Biophys Acta (BBA)-Mol Cell Biol Lipids 1864, 91–103.

Chouchani, E.T., and Kajimura, S. (2019). Metabolic adaptation and maladaptation in adipose tissue. Nat Metab 1, 189–200.

Cockcroft, S. (2001). Phosphatidylinositol transfer proteins couple lipid transport to phosphoinositide synthesis. Semin Cell Dev Biol 12, 183–191.

Cockcroft, S. (2012). The diverse functions of phosphatidylinositol transfer proteins. Curr Top Microbiol Immunol 362, 185–208.

Cockcroft, S., and Garner, K. (2011). Function of the phosphatidylinositol transfer protein gene family: is phosphatidylinositol transfer the mechanism of action? Crit Rev Biochem Mol Biol 46, 89–117.

Cockcroft, S., and Garner, K. (2012). 14-3-3 protein and ATRAP bind to the soluble class IIB phosphatidylinositol transfer protein RdgBβ at distinct sites. Biochem Soc Trans 40, 451–456.

Fromme, T., Kleigrewe, K., Dunkel, A., Retzler, A., Li, Y., Maurer, S., Fischer, N., Diezko, R., Kanzleiter, T., Hirschberg, V., et al. (2018). Degradation of brown adipocyte purine nucleotides regulates uncoupling protein 1 activity. Mol Metab 8, 77–85.

Garner, K., Hunt, A.N., Koster, G., Somerharju, P., Groves, E., Li, M., Raghu, P., Holic, R., and Cockcroft, S. (2012). Phosphatidylinositol transfer protein, cytoplasmic 1 (PITPNC1) binds and transfers phosphatidic acid. J Biol Chem 287, 32263–32276.

Glatz, J.F.C., and Luiken, J.J.F.P. (2018). Dynamic role of the transmembrane glycoprotein cd36 (sr-b2) in cellular fatty acid uptake and utilization. J Lipid Res 59, 1084–1093.

Grabon, A., Orłowski, A., Tripathi, A., Vuorio, J., Javanainen, M., Róg, T., Lönnfors, M., McDermott, M.I., Siebert, G., Somerharju, P., et al. (2017). Dynamics and energetics of the mammalian phosphatidylinositol transfer protein phospholipid exchange cycle. J Biol Chem 292, 14438–14455.

Gusarova, V., Brodsky, J.L., and Fisher, E.A. (2003). Apolipoprotein b100 exit from the endoplasmic reticulum (ER) is copii-dependent, and its lipidation to very low density lipoprotein occurs post-er. J Biol Chem 278, 48051–48058.

Halberg, N., Sengelaub, C.A., Navrazhina, K., Molina, H., Uryu, K., and Tavazoie, S.F. (2016). PITPNC1 recruits RAB1B to the golgi network to drive malignant secretion. Cancer Cell 29, 339–353.

Hammerschmidt, P., Ostkotte, D., Nolte, H., Gerl, M.J., Jais, A., Brunner, H.L., Sprenger, H.G., Awazawa, M., Nicholls, H.T., Turpin-Nolan, S. M., et al. (2019). CerS6-derived sphingolipids interact with Mff and promote mitochondrial fragmentation in obesity. Cell 177, 1536–1552. e23.

Hao, J.W., Wang, J., Guo, H., Zhao, Y.Y., Sun, H.H., Li, Y.F., Lai, X.Y., Zhao, N., Wang, X., Xie, C., et al. (2020). CD36 facilitates fatty acid uptake by dynamic palmitoylation-regulated endocytosis. Nat Commun 11, 4765.

Hernández-Alvarez, M.I., Sebastián, D., Vives, S., Ivanova, S., Bartoccioni, P., Kakimoto, P., Plana, N., Veiga, S.R., Hernández, V., Vasconcelos, N., et al. (2019). Deficient endoplasmic reticulum-mitochondrial phosphatidylserine transfer causes liver disease. Cell 177, 881–895.e17.

Hoffmann, L.S., Larson, C.J., and Pfeifer, A. (2016). cGMP and brown adipose tissue. Handb Exp Pharmacol 233, 283–299.

Hsuan, J., and Cockcroft, S. (2001). The PITP family of phosphatidylinositol transfer proteins. Genome Biol 2, reviews3011.1.

Hücking, K., Hamilton-Wessler, M., Ellmerer, M., and Bergman, R.N. (2003). Burst-like control of lipolysis by the sympathetic nervous system *in vivo*. J Clin Invest 111, 257–264.

Kahn, C.R., Wang, G., and Lee, K.Y. (2019). Altered adipose tissue and adipocyte function in the pathogenesis of metabolic syndrome. J Clin Invest 129, 3990–4000.

Kang, S. (2021). Adipose tissue malfunction drives metabolic dysfunction in Alström syndrome. Diabetes 70, 323–325.

Li, Y., Talbot, C.L., and Chaurasia, B. (2020). Ceramides in adipose tissue. Front Endocrinol 11, 407.

Litvak, V., Dahan, N., Ramachandran, S., Sabanay, H., and Lev, S. (2005). Maintenance of the diacylglycerol level in the golgi apparatus by the Nir2 protein is critical for golgi secretory function. Nat Cell Biol 7, 225–234.
Macher, G., Koehler, M., Rupprecht, A., Kreiter, J., Hinterdorfer, P., and Pohl, E.E. (2018). Inhibition of mitochondrial UCP1 and UCP3 by purine nucleotides and phosphate. Biochim Biophys Acta (BBA)-Biomembranes 1860, 664–672.
Mueez, U.D., Saari, T., Raiko, J., Kudomi, N., Maurer, S.F., Lahesmaa, M., Fromme, T., Amri, E.Z., Klingenspor, M., Solin, O., et al. (2018). Postprandial oxidative metabolism of human brown fat indicates thermogenesis. Cell Metab 28, 207–216.e3.
Mulder, P., Morrison, M.C., Verschuren, L., Liang, W., van Bockel, J.H., Kooistra, T., Wielinga, P.Y., and Kleemann, R. (2016). Reduction of obesity-associated white adipose tissue inflammation by rosiglitazone is associated with reduced non-alcoholic fatty liver disease in LDLr-deficient mice. Sci Rep 6, 31542.
Polyzos, S.A., Kountouras, J., and Mantzoros, C.S. (2017). Adipose tissue, obesity and non-alcoholic fatty liver disease. Minerva Endocrinol 42, 92–108.
Saraswathi, V., Kumar, N., Gopal, T., Bhatt, S., Ai, W., Ma, C., Talmon, G. A., and Desouza, C. (2020). Lauric acid versus palmitic acid: effects on adipose tissue inflammation, insulin resistance, and non-alcoholic fatty liver disease in obesity. Biology 9, 346.
Saxton, S.N., Clark, B.J., Withers, S.B., Eringa, E.C., and Heagerty, A.M. (2019). Mechanistic links between obesity, diabetes, and blood pressure: role of perivascular adipose tissue. Physiol Rev 99, 1701–1763.
Scheele, C., and Wolfrum, C. (2020). Brown adipose crosstalk in tissue plasticity and human metabolism. Endocrine Rev 41, 53–65.
Shadan, S., Holic, R., Carvou, N., Ee, P., Li, M., Murray-Rust, J., and Cockcroft, S. (2008). Dynamics of lipid transfer by phosphatidylinositol transfer proteins in cells. Traffic 9, 1743–1756.
Sigurdson, S.L., and Himms-Hagen, J. (1988). Control of norepinephrine turnover in brown adipose tissue of syrian hamsters. Am J Physiol 254, R960–R968.
Stephens, M., Ludgate, M., and Rees, D.A. (2011). Brown fat and obesity: the next big thing? Clin Endocrinol 74, 661–670.
Tan, Y., Shao, R., Li, J., Huang, H., Wang, Y., Zhang, M., Cao, J., Zhang, J., and Bu, J. (2020). PITPNC1 fuels radioresistance of rectal cancer by inhibiting reactive oxygen species production. Ann Transl Med 8, 126.
Tan, Y., Lin, K., Zhao, Y., Wu, Q., Chen, D., Wang, J., Liang, Y., Li, J., Hu, J., Wang, H., et al. (2018). Adipocytes fuel gastric cancer omental metastasis via PITPNC1-mediated fatty acid metabolic reprogramming. Theranostics 8, 5452–5468.
Turpin, S.M., Nicholls, H.T., Willmes, D.M., Mourier, A., Brodesser, S., Wunderlich, C.M., Mauer, J., Xu, E., Hammerschmidt, P., Brönneke, H. S., et al. (2014). Obesity-induced CerS6-dependent C16:0 ceramide production promotes weight gain and glucose intolerance. Cell Metab 20, 678–686.
Wang, J., Hao, J.W., Wang, X., Guo, H., Sun, H.H., Lai, X.Y., Liu, L.Y., Zhu, M., Wang, H.Y., Li, Y.F., et al. (2019). DHHC4 and DHHC5 facilitate fatty acid uptake by palmitoylating and targeting CD36 to the plasma membrane. Cell Rep 26, 209–221.e5.
Xu, D., Li, Y., Wu, L., Li, Y., Zhao, D., Yu, J., Huang, T., Ferguson, C., Parton, R.G., Yang, H., et al. (2018). Rab18 promotes lipid droplet (LD) growth by tethering the ER to LDs through SNARE and NRZ interactions. J Cell Biol 217, 975–995.
Ye, C., Duan, J., Zhang, X., Yao, L., Song, Y., Wang, G., Li, Q., Wang, B., Ai, D., Wang, C., et al. (2021). Cold-induced Yes-associated-protein expression through miR-429 mediates the browning of white adipose tissue. Sci China Life Sci 64, 404–418.
Zhang, X., Zhang, Y., Wang, P., Zhang, S.Y., Dong, Y., Zeng, G., Yan, Y., Sun, L., Wu, Q., Liu, H., et al. (2019). Adipocyte hypoxia-inducible factor 2α suppresses atherosclerosis by promoting adipose ceramide catabolism. Cell Metab 30, 937–951.e5.
Zhou, Z., Torres, M., Sha, H., Halbrook, C.J., Van den Bergh, F., Reinert, R.B., Yamada, T., Wang, S., Luo, Y., Hunter, A.H., et al. (2020). Endoplasmic reticulum-associated degradation regulates mitochondrial dynamics in brown adipocytes. Science 368, 54–60.

SUPPORTING INFORMATION

The supporting information is available online at https://doi.org/10.1007/s11427-022-2157-y. The supporting materials are published as submitted, without typesetting or editing. The responsibility for scientific accuracy and content remains entirely with the authors.